Nonlinear analysis of 3D reinforced concrete frames: effect of section torsion on the global response

Hamid R. Valipour*[1] and Stephen J. Foster[2a]

[1]*School of Civil and Environmental Engineering, University of Technology (UTS), Sydney, Australia*
[2]*School of Civil and Environmental Engineering, The University of New South Wales (UNSW), Sydney, Australia*

(Received October 22, 2009, Accepted July 10, 2010)

Abstract. In this paper the formulation of an efficient frame element applicable for nonlinear analysis of 3D reinforced concrete (RC) frames is outlined. Interaction between axial force and bending moment is considered by using the fibre element approach. Further, section warping, effect of normal and tangential forces on the torsional stiffness of section and second order geometrical nonlinearities are included in the model. The developed computer code is employed for nonlinear static analysis of RC sub-assemblages and a simple approach for extending the formulation to dynamic cases is presented. Dynamic progressive collapse assessment of RC space frames based on the alternate path method is undertaken and dynamic load factor (*DLF*) is estimated. Further, it is concluded that the torsional behaviour of reinforced concrete elements satisfying minimum standard requirements is not significant for the framed structures studied.

Keywords: concrete structures; dynamic analysis; frame; progressive collapse; softening.

1. Introduction

In 3D multi-story multi-bay reinforced concrete frames, cross sections can be subjected to normal (i.e., axial force and bending moment) and tangential (i.e., shear and torsion) forces, simultaneously. For coupling of these normal and tangential forces, three types of sectional models including fully coupled models (Bairan and Mari 2007), membrane models such as the modified compression field theory (MCFT) of Vecchio and Collins (1986) and the combination of them (Navarro Gregori *et al.* 2007) could be employed.

Progressive collapse is an important issue in structural failure, and has been since the partial collapse of the Ronan point apartment building in 1968. Since this time, a significant amount of research has been devoted to progressive collapse analysis of structures (Ellingwood and Leyendecker 1978, Khandelwal *et al*. 2008, Kim and Park 2008, Mohamed 2009, Yagob *et al*. 2009). One procedure for investigating potential for progressive collapse is based on alternative path method (APM), which has been integrated into several building codes (GSA 2003, DoD 2005), and adopted by different researchers for numerical modelling (Kaewkulchai and Williamson 2004, Bao

*Corresponding author, Senior Lecturer, E-mail: Hamid.Valipour@uts.edu.au
[a]Professor

et al. 2008). Moreover, APM procedures have been used by a few researchers for experimental study on progressive collapse (Sasani and Sagiroglu 2008b, Yi *et al*. 2008). In the APM approach, one or more columns are assumed to fail and are removed from the structural model with the remaining structure analysed to determine whether other members (or the structure) will fail or not.

The progressive collapse assessment of planar frames based on APM procedure has been focus of extensive studies (Kaewkulchai and Williamson 2004, Bao *et al*. 2008, Khandelwal *et al*. 2008, Yi *et al*. 2008), whereas only a few studies have been undertaken on the progressive collapse assessment of 3D frames and these studies mostly ignore the torsion effect at section level or adopt simplifying assumptions, such as reduced effective torsional stiffness, to take account of interaction between normal and tangential forces (Izzuddin *et al*. 2008, Sasani 2008, Sasani and Kropelnicki 2008, Mohamed 2009). On the other hand, some researchers have used continuum-based finite element models for collapse analysis of reinforced concrete framed structures subjected to abnormal loads such as blast, which are numerically very time-demanding (Gong *et al*. 2009, Weerheijm *et al*. 2009).

In undertaking of a space frame progressive collapse analyses, most models use linear elastic elements with lumped nonlinearity (Sasani 2008, Sasani and Sagiroglu 2008a, b). In this paper an element with distributed nonlinearity and formulated based on force interpolation concept and Navier-Bernoulli hypothesis is employed to capture the structure response. Obviously, by adopting the Navier-Bernoulli hypothesis the applicability of the formulation is limited to members with flexural behaviour, which is the case for most ordinary framed reinforced concrete structures, the focus of this paper. Moreover, a simple and efficient method based on a combination of the variable angle truss model and the modified compression field theory (MCFT) is used to establish the torque-twist relationship of a RC section, including the effect of interaction between tangential and normal forces. The developed element is used to study the effect of torsion on the potential progressive collapse of RC space frames.

2. Torque-twist curve of section subjected to pure torsion

The torque-twist curve for members in torsion reported in Valipour and Foster (2009b) is adopted in this paper with extension to cyclic loading. The curve is described briefly below. Test results on reinforced concrete members under pure torsion show that the torque-twist curve (Fig. 1) consists of four branches; line OA is a pre-cracking stage and point A corresponds to the cracking torsion; line AB shows the sudden jump in the section twist after cracking and the space truss analogy is used to capture point F; the position of point B is determined based on the tension stiffening concept and curve BC is taken to be parabolic; line CD, and the position of point D, is determined based on the concept of torsional ductility.

Thin-walled tube theory can be used to calculate the cracking torque T_{cr} (Hsu 1984)

$$T_{cr} = [1+(n-1)\rho]\left(\frac{A_c^2}{u_c}\right)f_{cr} \tag{1}$$

where A_c is the gross area of concrete, u_c is the perimeter of the concrete cross-section and f_{cr} denotes the cracking strength of concrete and is taken as equal to tensile strength of the concrete, f_t. The factor $[1+(n-1)\rho]$ on the right side of Eq. (1) takes account of the reinforcing steel on the cracking load, where ρ is the total volumetric ratio of the reinforcement and n is the modular ratio ($n = E_s/E_c$, where E_s and E_c are the elastic modulus of steel and concrete, respectively).

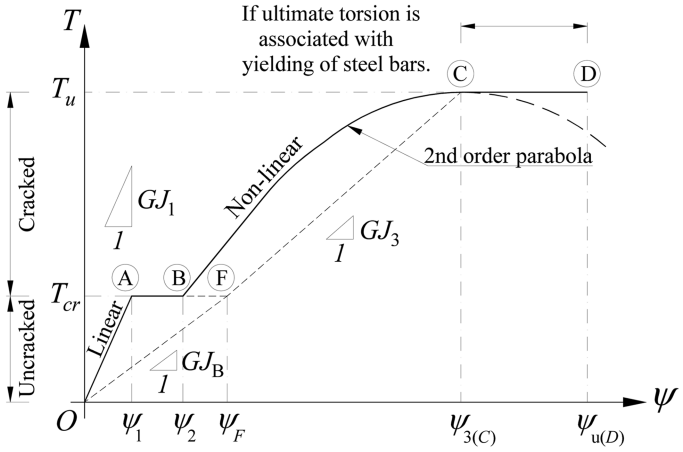

Fig. 1 Outline of the torque-twist curve for a section under pure torsion

Adopting the Saint-Venant's theory of elastic torsion for a rectangular section of height h, and width w, gives the section torsional constant J_1 as (Young and Roark 2001)

$$J_1 \cong wh^3\left[\frac{1}{3}-0.21\frac{h}{w}\left(1-\frac{h^4}{12w^4}\right)\right] \quad (h \le w) \tag{2}$$

and the twist ψ_1, at the point of cracking point is then calculated from

$$\psi_1 = \frac{T_{cr}}{G_c J_1} \tag{3}$$

where G_c is the shear modulus of concrete and is taken as $G_c = E_c/2(1+\nu)$ and ν is the Poisson's ratio.

According to the space truss analogy, after full torsional cracking, the reinforcing steel controls the stiffness and torsion is resisted by a truss action of compressive struts and tensile stresses in reinforcement (Hsu 1984), with no shear transferred along the crack surface. For the analysis of RC solid members, the solid section must be substituted with a hollow section of effective thickness, t_e, and the bars are assumed to be distributed evenly over the section perimeter.

Adopting the thin-walled tube theory of torsion, for the equivalent hollow section, and satisfying the equilibrium of the horizontal and vertical forces, for a typical element taken from the walls of the equivalent hollow section gives (Rahal and Collins 1996)

$$T = 2A_o\sqrt{\frac{A_l f_l}{u_o}\frac{A_t f_t}{s}}, \quad u_o = u_c - 4a_0, \quad A_o = (w-a_0)(h-a_0) \tag{4}$$

$$\tan\theta = \sqrt{\frac{A_t f_t}{s}\frac{u_o}{A_l f_l}} \tag{5}$$

where a_0 is the thickness of the equivalent compressive struts, A_o is the effective area of the equivalent cross section, u_o is the effective perimeter of the cross section (Fig. 2), f_l and f_t denote the stress in longitudinal and transverse reinforcing steel, respectively, A_l is the total area of longitudinal reinforcement, A_t is the area of one leg of a transverse steel bar, s is the average

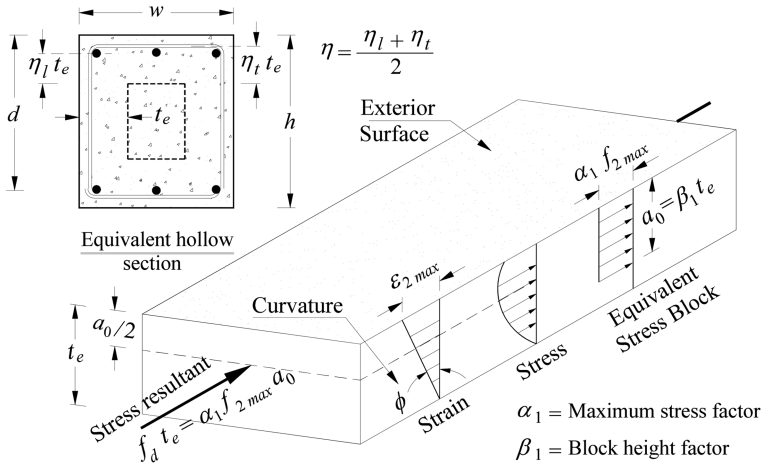

Fig. 2 Outline of a concrete strut and equivalent rectangular stress block

spacing of transverse reinforcing and θ is the inclination angle of the compressive struts with respect to element longitudinal axis. The torsional constant J_h for the thin walled tube is

$$J_h = 4t_e(A_o^2/u_o) \tag{6}$$

The position of the key points (i.e., A, B, C and D) on the torque-twist curve (see Fig. 1) can be obtained by defining appropriate values for A_o and u_o in Eqs. (4) and (5), and is explained in the following sections.

Point A in Fig. 1 represents the first cracking and point F represents the fully cracked state and the corresponding torsional stiffness can be obtained by adopting the Collins and Lampert (1971) approach. This implies that the torsional stiffness is approximately that of a tube with the same dimensions and an effective wall thickness of $t_e = \sqrt{(A_l/u_o)(A_t/s)}$. Accordingly, the torsional stiffness, GJ_F, and corresponding twist, ψ_F, can be calculated by adopting the area enclosed by the stirrup centrelines as being the effective area. Substituting t_e into Eq. (6) gives

$$GJ_F = 4G_s\left(\frac{A_h^2}{u_h}\right)\sqrt{\frac{A_t}{s}\cdot\frac{A_l}{u_h}} \tag{7}$$

$$\psi_F = \frac{T_{cr}}{GJ_F} \tag{8}$$

where G_s is the elastic shear modulus of the steel bars and A_h and u_h denote the area and perimeter bounded by centreline of the stirrups, respectively.

In Eq. (7) the torsional stiffness of the cracked section is calculated by taking account of the reinforcing steel stiffness and ignoring the influence of the concrete between the cracks. This leads to an underestimation of section stiffness and can, in part, be attributed to the tension-stiffening effect. A simple approach, inspired from the modified stress-strain relationship of steel proposed by CEB-FIP model code 1990, is used to take account of this tension stiffening. In the model used in this study, the twist at point B can be obtained from

$$\psi_2 = \lambda\psi_1 + (1-\lambda)\psi_F \quad \text{where} \quad \lambda = 0.6 - 0.2/\exp(1000\rho_t) \tag{9}$$

where ρ_t is the ratio of transverse reinforcement and λ is a multiplier between 0.4 and 0.6 (Valipour 2009, Valipour and Foster 2009b).

Based on Lampert and Thurlimann's (1968) method the ultimate torsional capacity of the section (point C in Fig. 1) can be determined by assuming that the concrete within the core, that is at a depth greater than t_e from the surface, is virtually unstressed and the principal compressive strain over the effective strut thickness varies linearly with the highest strain at the exterior surface, as shown in Fig. 2 (Mitchell and Collins 1974). The wall thickness of the equivalent hollow section, a_0, is calculated based on an equivalent rectangular stress block (see Fig. 2) and the stress resultant in the compressive strut is obtained from

$$f_d t_e = \alpha_1 f_{2\max} a_0 \tag{10}$$

where $f_{2\max}$ is the maximum compressive strength of diagonally cracked concrete and $\alpha_1 = 0.9$. Further

$$f_{2\max} = S f_{cp} \tag{11}$$

$$0.4 \le S = \frac{1}{0.8 + 170\varepsilon_1} \le 1.0 \tag{12}$$

where f_{cp} is the concrete compressive strength, S is a compressive strength reduction factor for the concrete strut according to the modified compression field theory (MCFT) and ε_1 is the average tensile strain normal to the direction of the struts and is a function of load and the strut orientation.

Re-writing the truss model equations derived in the previous section with consideration to the MCFT yields

$$\frac{A_l f_l}{u_o} + \frac{A_t f_t}{s} = \alpha_1 f_{2\max} a_0 = \alpha_1 f_{2\max} \beta_1 t_e, \quad u_o = 2(h + w - 2a_0) \tag{13}$$

$$\beta_1 = \begin{cases} 0.85 & f_{cp} \le 28 \\ 0.85 - 0.007(f_{cp} - 28) & 28 \le f_{cp} \end{cases} \tag{14}$$

In Eqs. (13) and (14) the equivalent rectangular compressive block height for normal strength concrete is calculated by using a factor taken from AS-3600 (2009). It is noteworthy that the state of stress in concrete and steel is unknown and Eq. (13) needs to be solved iteratively.

Using strain compatibility equations, Mitchell and Collins (1974) showed that

$$\phi = \psi \sin 2\theta \tag{15}$$

where ϕ is the transverse curvature of a concrete strut (see Fig. 2) and ψ is the section twist angle. From linear strain distribution over the strut thickness, and Eq. (15), we have

$$\psi = \psi_{3(C)} = \frac{\varepsilon_{2\max}}{t_e \sin 2\theta} \tag{16}$$

where $\varepsilon_{2\max}$ can be obtained based on the CFT approach of (Rahal and Collins 1996) and is given by

$$\varepsilon_{2\max} = 1.5S\varepsilon_{c0} \tag{17}$$

and where ε_{c0} is the strain corresponding with uniaxial compressive strength of the concrete and S can be obtained from Eq. (12). Finally, having calculated θ, t_e and $\varepsilon_{2\max}$, the twist corresponding with point C on the torque-twist curve in Fig. 1 can be obtained from Eq. (16).

If the ultimate torsional capacity corresponding to point C in Fig. 1 is associated with yielding of the steel, the failure mode is taken to be ductile and a value of $\psi_D = 1.5\,\psi_C$ is used to construct the CD branch of the torque-twist curve. Otherwise, it is taken that the failure mode is non-ductile and the CD plateau (see Fig. 1) in the torque-twist curve does not exist.

3. Strain in the longitudinal and transverse steel

With regard to experimental results (Hsu 1984), it is assumed that the longitudinal and transverse bars are strained just beyond point A and that over branch OA the strain caused by torsion in the reinforcing bars is negligible. Moreover, it is assumed that the variation of strain with respect to section twist follows a linear function. Accordingly, if the twist and strain $\varepsilon_{3l(3t)}$ corresponding to point C are known, the strain can be obtained by

$$\varepsilon_{l(t)} = \varepsilon_{3l(3t)}(\psi - \psi_A)/(\psi_C - \psi_A) \tag{18}$$

where $\varepsilon_{l(t)}$ represents the strain in the longitudinal (transverse) reinforcement.

Using the truss model compatibility equations, the strain in the longitudinal and transverse bars corresponding to ultimate torque (point C in Fig. 1) can be obtained from (Hsu 1984) as

$$\varepsilon_{3l} = \left(\frac{\alpha_1\beta_1 A_o^2 f_{2\max}}{T_u u_o \cot\theta} - \eta\right)\varepsilon_{2\max} \tag{19}$$

$$\varepsilon_{3t} = \left(\frac{\alpha_1\beta_1 A_o^2 f_{2\max}}{T_u u_o \tan\theta} - \eta\right)\varepsilon_{2\max} \tag{20}$$

where η is the average of η_l and η_t defined in Fig. 2. Similar relationships in terms of reinforcing steel bars area and stresses have been derived by Rahal and Collins (1996).

4. Interaction of tangential and normal forces

Application of interaction diagrams is an efficient and reasonably accurate tool to determine the ultimate capacity of a section under combined forces. The interaction diagram does not, however, define the variation of section stiffness at different states and, consequently, is not applicable for practical analysis of statically indeterminate framed structures. By adopting some simple assumptions consistent with principles of the truss model, the torque-twist curve of a section under pure torsion developed in Section 2 is modified to construct the torque-twist relationship for a section subjected to a combination of tangential and normal forces. The outline of the modified torque-twist curve, compared with the original torque-twist curve, is shown in Fig. 3.

The first assumption is that the initial cracking torque is only affected by the bending moment and axial force. This is not completely correct for members experiencing some level of cracking due to

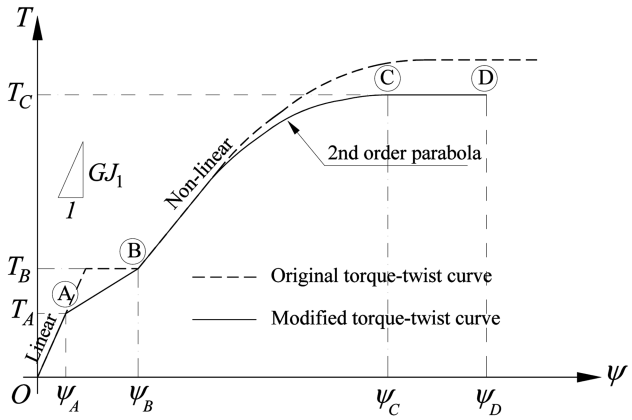

Fig. 3 Outline of the torque-twist curve for a section under torsion, axial force and bending moment

shear, such as thin-walled hollow sections, but this effect is limited to early stage of the response and has only a minor effect on the ultimate capacity. With regard to this assumption, axial and flexural cracks of width (w) greater than five times characteristic crack width (w_{ch}), where $w_{ch} = G_f/f_t$ and where G_f is the fracture energy and f_t is the tensile strength of concrete (Cornelissen *et al*. 1986), do not contribute to the torsional strength of the member. The initial cracking torque, T_A, is then calculated as

$$T_A = [1+(n-1)\rho]\left(\frac{A_{c_{eff}}^2}{u_{c_{eff}}}\right)f_{cr} \tag{21}$$

where $A_{c_{eff}}$ and $u_{c_{eff}}$ are the effective area and perimeter of the cracked section, respectively.

The twist corresponding to point A is obtained by assuming that the stiffness of the section before initial cracking remains unchanged (J_1 is obtained from uncracked geometry). Hence

$$\psi_A = \frac{T_A}{G_c J_1} \tag{22}$$

The second assumption is that the value of the full cracking torque, $T_B = T_{cr}$, is not affected by other forces (see Fig. 3), while the twist corresponding to point B is calculated from

$$\psi_B = \lambda\psi_A + (1-\lambda)\psi_F \tag{23}$$

where ψ_F is calculated according to the procedure outlined in Section 2.

The effect of normal forces on the ultimate torque, T_u, is considered by reducing the total area of longitudinal bars and defining the effective area of longitudinal bars $A_{l_{eff}}$ based on the ultimate tensile strength of the longitudinal bars. If n denotes the number of longitudinal bars and A_{l_i} and f_{u_i} denote the area and ultimate strength of longitudinal bar i, respectively, the effective area of longitudinal bars, $A_{l_{eff}}$, can be obtained from

$$A_{l_{eff}} = \frac{\sum_{i=1}^{n} A_{l_i}(f_{u_i}-f_{s_i})}{\sum_{i=1}^{n} A_{l_i} f_{u_i}} A_l \tag{24}$$

and where f_{s_i} is the stress in bar i caused by any co-existing normal forces. Accordingly, when the ultimate torsional capacity of a section and corresponding twist are calculated, the value of A_l in Eqs. (4), (5) and (13) is replace by $A_{l_{eff}}$.

The shear effect on the ultimate torsional capacity is taken into account by a direct approach inspired from torque-shear interaction relationships. Among the applicable shear-torsion interaction equations that are available in the literature, the elliptical form of (Klus 1968) is adopted in this study. The ultimate torque, T_C, and corresponding twist, ψ_C, are then calculated from

$$T_C = T_u\sqrt{1-(V/V_u)^2} \tag{25}$$

$$\psi_C = \psi_u\sqrt{1-(V/V_u)^2} \tag{26}$$

where T_u and ψ_u are the ultimate torque and twist calculated based on $A_{l_{eff}}$, respectively.

In this study the ultimate shear strength of a section, V_u, is obtained from AS-3600 (2009) as

$$V_u = V_{u\,\min} + (A_{sv} f_{yt} d/s)\cot\theta_v \tag{27}$$

$$V_{u\,\min} = \beta_1\beta_2 wd\left(\frac{A_{st} f_{cp}}{wd}\right)^{1/3} \tag{28}$$

$$V_{u\,\max} = 0.2 f_{cp} wd \tag{29}$$

$$\theta_v = \left(2 + \frac{V - V_{u\,\min}}{V_{u\,\max} - V_{u\,\min}}\right)(15^{\circ}) \quad \text{in degrees} \tag{30}$$

where A_{st} is the cross sectional area of fully anchored longitudinal reinforcement provided in the tensile zone, A_{sv} is the cross sectional area of the shear reinforcement, d is the section effective depth, θ_v is the angle between concrete compressive struts and the longitudinal axis of the member, which is interpolated between 30° to 45° depending on shear force level. Further, $\beta_1 = 1.1(1.6 - d/1000) \geq 1.1$ is a factor taking account of section size, β_2 is a factor taking account of axial force and for members subjected to significant compression $\beta_2 = 1 + N/14A_g$. For members under axial tension $\beta_2 = 1 - N/3.5A_g \geq 0$, where N and A_g denote the axial force and section gross area, respectively.

It is noteworthy that the simple shear model adopted in this formulation can capture the possible shear failure in case it dominates the response and the interaction between shear and torsion with reasonable accuracy. The shear deformation, however, is not taken into account which of course is not that significant for ordinary frame elements with the span to depth ratio of more than 4 as the main focus of this paper.

The outline of the flowchart and adopted algorithm for constructing the modified torque-twist curve can be found in Valipour (2009).

5. Total secant formulation of element

Fig. 4(a) shows a 2-node frame element AB with 3 translational and 3 rotational DOFs. If the torsional degrees of freedom are taken to be uncoupled from the other DOFs, the total form of the equilibrium equation for configuration Ax after deformation (see Fig. 4b), yields

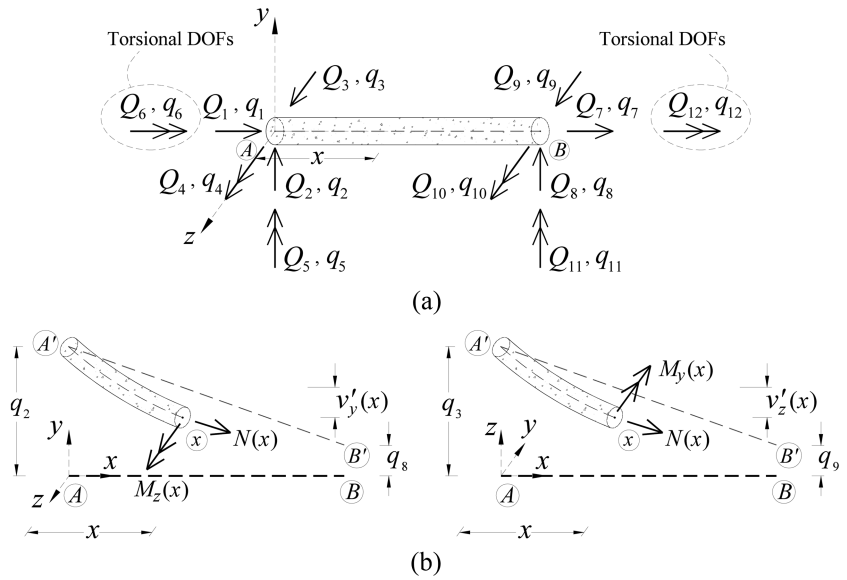

Fig. 4 (a) 2-node frame element *AB*, (b) Projection of deformed configuration *Ax*, in *x*-*y* and *x*-*z* plane

$$\mathbf{D}(x) = \mathbf{b}(x)\mathbf{Q}_A + \mathbf{D}^*(x) + \mathbf{D}_{\text{und}}(x) \tag{31}$$

$$\mathbf{b}(x) = \begin{bmatrix} -1 & 0 & 0 & 0 & 0 \\ 0 & x & 0 & -1 & 0 \\ 0 & 0 & -x & 0 & -1 \end{bmatrix} \tag{32}$$

where $\mathbf{b}(x)$ is the force interpolation matrix, $\mathbf{Q}_A = [Q_1 \;\; Q_2 \;\; Q_3 \;\; Q_4 \;\; Q_5]^T$ is the vector of nodal generalised force (without torsional DOF) at end A, $\mathbf{D}(x)$ is a vector of total section internal forces, $\mathbf{D}^*(x) = [P^*(x) \;\; M_z^*(x) \;\; M_y^*(x)]^T$ is a vector of total section forces solely due to the element loads and $\mathbf{D}_{\text{und}}(x) = [0 \;\; Q_1 v_y'(x) \;\; Q_1 v_z'(x)]^T$ refers to the undulation effect, which is the deflection of the element with respect to the rotated axis of the element after deformation (Carol and Murcia 1989).

Adopting a perfect bond assumption and the Navier-Bernoulli hypothesis, the total normal strain of the fibres in local *x*-*x* direction, $\varepsilon(x)$, can be obtained from

$$\varepsilon(x) = \varepsilon_{N-B} + \varepsilon_W = \varepsilon_r(x) - y\kappa_z(x) - z\kappa_y(x) + \varepsilon_W \tag{33}$$

where ε_{N-B} denotes the component of strain related to axial force and bending, based on the Navier-Bernoulli assumption and $\varepsilon_r(x), \kappa_z(x)$ and $\kappa_y(x)$ are the section total axial strain and curvatures about local *z*- and *y*-axes, respectively, and ε_W denotes the torsion related strain component and it is only non-zero for fibres in the equivalent box domain Ξ (see Fig. 2).

Decomposing the total strain to elastic, ε_e, and inelastic, ε_p, components, the constitutive law can be expressed in the total secant form (Fig. 5)

$$\sigma = E_e(\varepsilon - \varepsilon_p) \tag{34}$$

where E_e is the total secant modulus of the unloading curve.

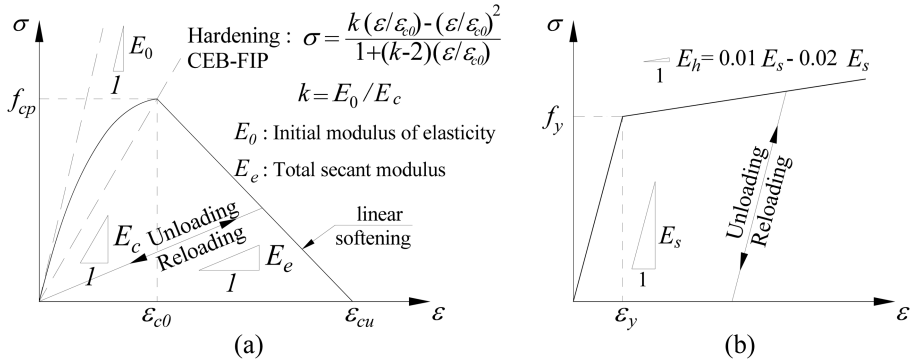

Fig. 5 (a) CEB-FIP model for compressive concrete (hardening) with linear softening, (b) bi-linear stress-strain relationship adopted for steel bars

The complete stress-strain relationship of concrete and steel bars, together with unloading/ reloading rules adopted in this paper, is shown in Fig. 5. Since the softening of concrete under tension and compression is taken into account the constitutive law scaling approach is adopted to restore the objectivity of results (Coleman and Spacon 2001).

Substituting Eqs. (33) and (34) into section equilibrium equations, yields

$$\mathbf{D}(x) = {}^{e}\mathbf{k}_s(x)\mathbf{d}(x) + \mathbf{D}_p(x) - \mathbf{D}_W(x) \tag{35}$$

$${}^{e}\mathbf{k}_s(x) = \begin{bmatrix} \int_\Omega E_e dA & -\int_\Omega y E_e dA & -\int_\Omega z E_e dA \\ -\int_\Omega y E_e dA & \int_\Omega y^2 E_e dA & \int_\Omega yz E_e dA \\ -\int_\Omega z E_e dA & \int_\Omega yz E_e dA & \int_\Omega z^2 E_e dA \end{bmatrix} \tag{36}$$

$$\mathbf{D}_p(x) = [-\int_\Omega E_e \cdot \varepsilon_p dA \quad \int_\Omega y E_e \cdot \varepsilon_p dA \quad \int_\Omega z E_e \cdot \varepsilon_p dA]^T \tag{37}$$

$$\mathbf{D}_W(x) = [-\int_\Xi E_e \cdot \varepsilon_W dA \quad \int_\Xi y E_e \cdot \varepsilon_W dA \quad \int_\Xi z E_e \cdot \varepsilon_W dA]^T \tag{38}$$

where ${}^{e}\mathbf{k}_s(x)$ is the secant stiffness matrix of the section, $\mathbf{D}_p(x)$ is the residual plastic force vector for the section, $\mathbf{D}_W(x)$ is the section force vector due to torsion-warping and $\mathbf{d}(x) = [\varepsilon_r(x) \ \kappa_z(x) \ \kappa_y(x)]^T$ is the generalized total strain vector of the section. The secant flexibility matrix of the section, ${}^{e}\mathbf{f}_s(x)$, is obtained by inverting the section secant stiffness matrix and then Eq. (35) can be rearranged as

$$\mathbf{d}(x) = {}^{e}\mathbf{f}_s(x)\{\mathbf{D}(x) - \mathbf{D}_p(x) + \mathbf{D}_W(x)\} \tag{39}$$

The section integrals in Eqs. (36) to (38) are calculated numerically by fibre element discritisation.

If ${}^{e}\mathbf{K}_e$ and k_τ denote the secant stiffness matrix and torsional stiffness of the element AB, respectively, adopting the torsions as independent of the other forces, we have

$$ {}^{e}\mathbf{K}_{e} = \begin{bmatrix} {}^{e}\mathbf{K}_{AA} & \mathbf{0} & {}^{e}\mathbf{K}_{AA}\Gamma & \mathbf{0} \\ \mathbf{0} & k_{\tau} & \mathbf{0} & k_{\tau} \\ \Gamma^{e}\mathbf{K}_{AA} & \mathbf{0} & \Gamma^{T\,e}\mathbf{K}_{AA}\Gamma & \mathbf{0} \\ \mathbf{0} & k_{\tau} & \mathbf{0} & k_{\tau} \end{bmatrix} \tag{40} $$

$$ \Gamma = -\begin{bmatrix} & 0 & 0 \\ \mathbf{I}_{3\times 3} & -L & 0 \\ & 0 & L \\ \mathbf{0}_{2\times 3} & \mathbf{I}_{2\times 2} & \end{bmatrix}, \quad \mathbf{I}\text{: Identity matrix} \tag{41} $$

Applying the virtual work principle for the cantilever configuration AB that is subjected to a virtual load vector at the free end, then from Eqs. (31) and (39) (Valipour 2009)

$$ {}^{e}\mathbf{K}_{e}\mathbf{q} = \mathbf{Q} - \mathbf{Q}_{p} + \mathbf{Q}_{W} + \mathbf{Q}^{*} - \mathbf{Q}^{*}_{end} + \mathbf{Q}_{\text{und}} - \mathbf{Q}_{P-\Delta} \tag{42} $$

$$ {}^{e}\mathbf{K}^{-1}_{AA} = {}^{e}\mathbf{F}_{AA} = \int_{0}^{l} \mathbf{b}^{T}(x)\,{}^{e}\mathbf{f}_{s}(x)\mathbf{b}(x)dx \tag{43} $$

$$ \mathbf{Q}_{\alpha} = [{}^{e}\mathbf{K}_{AA}\mathbf{q}_{\alpha(A)} \;\; 0 \;\; \Gamma^{T\,e}\mathbf{K}_{AA}\mathbf{q}_{\alpha(A)} \;\; 0]^{T}, \quad \alpha = p, W, \text{und} \tag{44} $$

$$ \mathbf{Q}^{*} = [{}^{e}\mathbf{K}_{AA}\mathbf{q}^{*}_{(A)} \;\; 0 \;\; \Gamma^{T\,e}\mathbf{K}_{AA}\mathbf{q}^{*}_{(A)} \;\; 0]^{T} \tag{45} $$

$$ \mathbf{Q}^{*}_{end} = [\mathbf{0}_{1\times 5} \;\; 0 \;\; \mathbf{R}_{B} \;\; 0]^{T} \tag{46} $$

$$ \mathbf{Q}_{P-\Delta} = [\mathbf{Q}_{P-\Delta(A)} \;\; 0 \;\; -\mathbf{Q}_{P-\Delta(A)} \;\; 0]^{T} \tag{47} $$

$$ \mathbf{q}_{\alpha(A)} = \int_{0}^{l} \mathbf{b}^{T}(x)\,{}^{e}\mathbf{f}_{s}(x)\mathbf{D}_{\alpha}(x)dx, \quad \alpha = p, W, \text{und} \tag{48} $$

$$ \mathbf{q}^{*}_{(A)} = \int_{0}^{l} \mathbf{b}^{T}(x)\,{}^{e}\mathbf{f}_{s}(x)\mathbf{D}^{*}(x)dx \tag{49} $$

where, ${}^{e}\mathbf{F}_{AA}$ and ${}^{e}\mathbf{K}_{AA}$ are the flexibility and stiffness sub-matrix of end A, $\mathbf{q}_{p(A)}$ denotes the nodal generalised plastic deformation at end A, $\mathbf{q}_{W(A)}$ is the generalised displacement at end A due to torsional warping, $\mathbf{q}^{*}_{(A)}$ is the vector of nodal generalised deformation at end A due to element loads and $\mathbf{q}_{\text{und}(A)}$ is a vector of nodal generalised deformations due to the undulation effect. The vector $\mathbf{Q}_{P-\Delta(A)} = [0 \;\; Q_1(q_8 - q_2)/l \;\; Q_1(q_9 - q_3)/l \;\; 0 \;\; 0]^{T}$ is a vector of generalised nodal forces at end A due to P-Δ effects, $\mathbf{Q}^{*}_{end}$ is a vector containing the end nodal forces due to element distributed load, $\mathbf{R}_{B} = [R_1 \;\; R_2 \;\; R_3 \;\; R_4 \;\; R_5]^{T}$ is the reaction vector at clamped end B due to element load and $\mathbf{0}_{1\times 5}$ is a 1 by 5 null matrix.

Since in the force-based element no displacement shape function is used, a more elaborate approach is needed when compared to displacement-based approach for updating the element (structure) deflected shape. Adopting the small strains and slope within the Navier-Bernoulli beam theory leads to the following strain-displacement relationships for an arbitrary section located at

distance x along the element axis projected in x-y (x-z) plane (Fig. 4)

$$v_y'(x) = \{(q_8 - q_2)/l - q_4\}x - \int_0^x (x-s)\kappa_z(s)ds \tag{50}$$

$$v_z'(x) = \{(q_9 - q_3)/l - q_5\}x - \int_0^x (x-s)\kappa_y(s)ds \tag{51}$$

In this study, a composite Simpson integration method is employed to numerically determine the integrals along the element axis (Valipour and Foster 2008). Using the composite Simpson's scheme, the integrals on the right side of Eqs. (50) and (51) can be easily calculated for the odd numbered longitudinal sections. For the even numbered sections, a piecewise parabolic interpolation of curvature function is used. A Simpson scheme with ($2n$ + 1) integration point along the element divides the element to n equal sub-elements. If it is assumed that the curvature varies parabolically along each sub-element, then integrals in Eqs. (50) and (51) can be calculated analytically for the even numbered sections.

It was determined in Valipour and Foster (2008) that the total secant solution method offers better stability compared with the tangent approach and can handle the stress-strain relationships that have a horizontal plateau, such as the torque-twist adopted in this study.

6. Modified torque-twsit curve for cyclic loading

The modified sectional torque-twist curve, together with predefined variation of strain in steel bars, constructs the framework for cyclic torque-twist relationship (see Fig. 6). With regard to Fig. 6, and consistent with the damage model adopted for the concrete material, it is assumed that the unloading/reloading branch before the reinforcement yielding (point (ψ_y, T_y) in Fig. 6) follows from the total secant modulus. After yielding of the reinforcement, the unloading/reloading branch follows a line with a slope equal to the initial modulus of the torque-twist curve and full unloading is based on the concept of kinematic hardening.

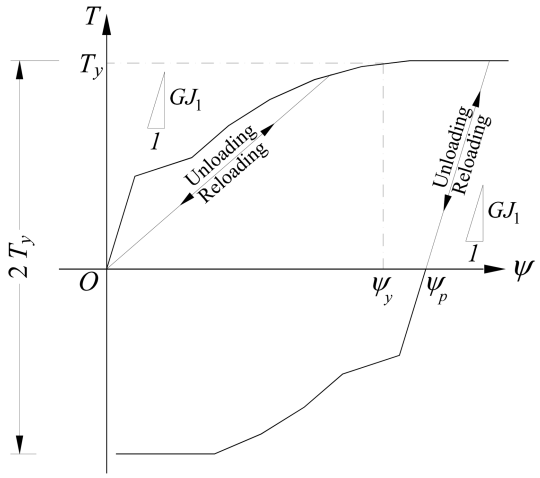

Fig. 6 Unloading/reloading rules for cyclic torque-twist curve

If ψ_p denotes the plastic twist, the section torque-twist after yielding can be re-written as

$$T = GJ_1(\psi - \psi_p) \tag{52}$$

Accordingly, the element plastic force vector, $\mathbf{Q}_p$, given in Eq. (44) is modified as follows

$$\mathbf{Q}_p = [{}^e\mathbf{K}_{AA}\mathbf{q}_{p(A)} \;\; k_\tau\omega_p \;\; \Gamma^T {}^e\mathbf{K}_{AA}\mathbf{q}_{p(A)} \;\; -k_\tau\omega_p]^T \tag{53}$$

where $\omega_p = -\int_0^l \psi_p \, dx$ denotes the element plastic deformation due to torsion and k_τ is the element torsional stiffness.

The cyclic torque-twist relationship shown in Fig. 6 is overly simplified for cases in which a frame element is subjected to high range of unloading/reloading cycles, such as seismic loadings. However, for the potential progressive collapse analysis of frames, where just the first few unloading/reloading cycles are important, the model performance appears reasonable for capturing the global response of a structure.

7. Implementation of the formulation for dynamic analysis

The recursive total form of the dynamic equilibrium equations for a disretised system at the instant $t + \Delta t$ is

$$\mathbf{M}_{\text{St.}} {}^{t+\Delta t}\ddot{\mathbf{q}}_{\text{St.}}^{(i)} + \mathbf{C}_{\text{St.}} {}^{t+\Delta t}\dot{\mathbf{q}}_{\text{St.}}^{(i)} + \mathbf{K}_{\text{St.}}^{(i-1)} {}^{t+\Delta t}\mathbf{q}_{\text{St.}}^{(i)} = {}^{t+\Delta t}\mathbf{F}_{\text{St.}}^{(i)} \tag{54}$$

$${}^{t+\Delta t}\mathbf{F}_{\text{St.}}^{(i)} = {}^{t+\Delta t}\mathbf{R}_{\text{St.}} - \sum \mathbf{Q}_p^{(i-1)} + \sum \mathbf{Q}_W^{(i-1)} + \sum \mathbf{Q}^{*(i-1)} - \sum \mathbf{Q}_{end}^{*(i-1)} + \sum \mathbf{Q}_{\text{und}}^{(i-1)} - \sum \mathbf{Q}_{P-\Delta}^{*(i-1)} \tag{55}$$

where $\mathbf{M}_{\text{St.}}, \mathbf{C}_{\text{St.}}$ and $\mathbf{K}_{\text{St.}}^{(i-1)}$ are the mass, damping and total secant stiffness matrices of the structure with superscript $(i-1)$ denoting the iteration number, ${}^{t+\Delta t}\mathbf{R}_{\text{St.}}$ is the external nodal force vector and ${}^{t+\Delta t}\mathbf{q}_{\text{St.}}^{(i)}$, ${}^{t+\Delta t}\dot{\mathbf{q}}_{\text{St.}}^{(i)}$ and ${}^{t+\Delta t}\ddot{\mathbf{q}}_{\text{St.}}^{(i)}$ denote displacement, velocity and acceleration vectors of the structure, respectively. After time discretisation of Eq. (54) using a standard method such as the Newmark or θ-Wilson (Bathe 1997), the recursive equations are solved by following a direct iterative scheme (Valipour and Foster 2009a).

In the numerical examples presented in this paper, wherever required, a proportional damping in the form of $\mathbf{C}_{\text{St.}} = a\mathbf{M}_{\text{St.}} + b\mathbf{K}_{\text{St.}}$ is adopted.

8. Numerical examples

8.1 Introduction

In this section four numerical examples are used to demonstrate the performance of the model, assess its accuracy and determine the importance of including the modelling of torsion in assessing the structure response of 3D regular building frames. Further to the examples presented below, the reader is referred to (Valipour and Foster 2009b) and (Valipour 2009) demonstrating the validity of the static torsional model for various beam-beam sub-assemblages subjected to various combinations of bending, shear and torsion.

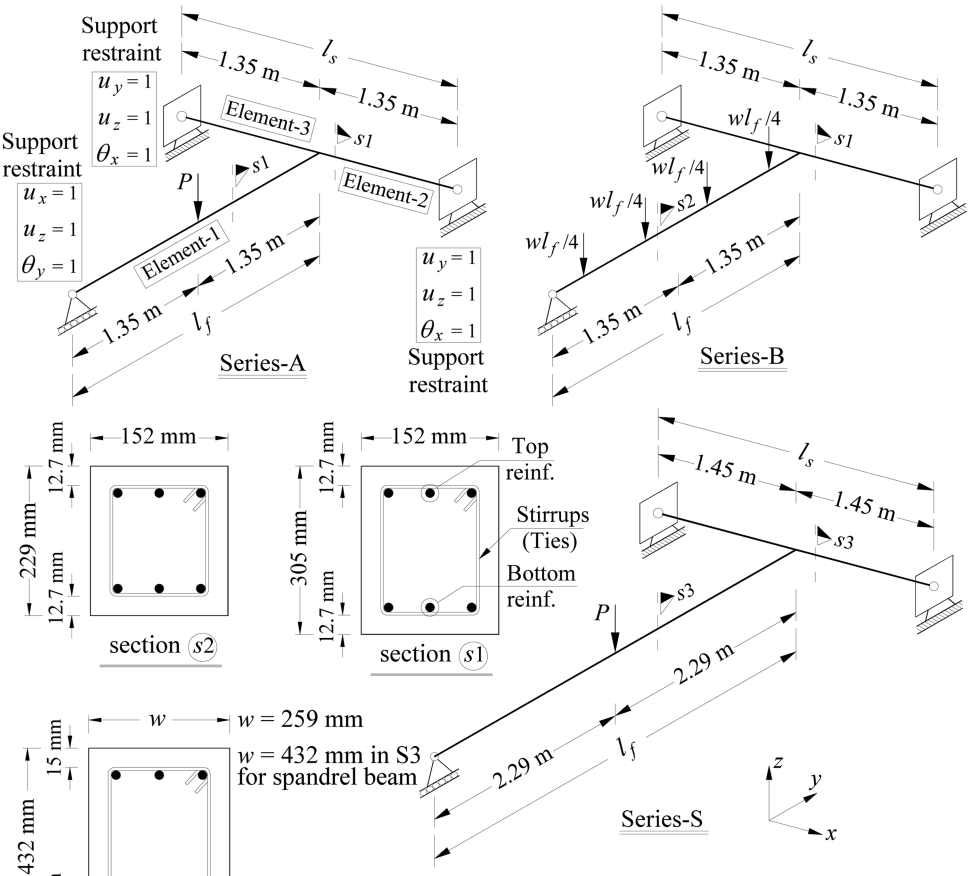

		Floor beam		Spandrel beam	f_{cp} (MPa)	E_0 (MPa)	f_y^* (MPa)
		Mid span	End span				
A3	Top	2 ϕ9.5	2 ϕ9.5	2 ϕ6.5	38.2	35	ϕ6.5 : 348
	Stirrups	ϕ6.5@89 mm	ϕ6.5@89 mm	ϕ6.5@121 mm			ϕ9.5 : 475
	Bottom	3 ϕ19	2 ϕ19	2 ϕ16 +1 ϕ9.5			
B2	Top	2 ϕ6.5	2 ϕ9.5	2 ϕ6.5	28.4	27	ϕ6.5 : 345
	Stirrups	ϕ6.5@102 mm	ϕ6.5@102 mm	ϕ6.5@127 mm			ϕ9.5 : 481
	Bottom	2 ϕ16 +1 ϕ9.5	2 ϕ16	2 ϕ16			
S1	Top	2 ϕ16	2 ϕ16	2 ϕ16	24.1	24	ϕ6.5 : 310
	Stirrups	ϕ6.5@190 mm	ϕ6.5@190 mm	ϕ9.5@108 mm			ϕ9.5 : 294
	Bottom	2 ϕ25.4	2 ϕ25.4	4 ϕ16			ϕ12.7 : 293
S3	Top	4 ϕ16	4 ϕ16	2 ϕ16	24.1	24	ϕ16 : 434
	Stirrups	ϕ6.5@190 mm	ϕ6.5@190 mm	ϕ9.5@137 mm			ϕ25.4 : 403
	Bottom	6 ϕ16	6 ϕ16	5 ϕ16			

Note * : Steel initial moduls of elasticity is $E_s = 200$ (GPa) and $E_h = 0.01\,E_s$.

Fig. 7 Outline of the T-specimens, section and reinforcing details for Hsu and Burton (1974) and Collins and Lampert (1971) tests

8.2 Nonlinear analysis of T sub-assemblages

In this example, the T-specimens taken from Hsu and Burton (1974) and Collins and Lampert (1971) tests are analysed. The geometry of the specimens and sections, the reinforcing details, loadings and material properties are given in Fig. 7. The tensile strength of concrete is taken as $f_t = 0.33\sqrt{f_{cp}}$ and the strain corresponding to the compressive strength of concrete is $\varepsilon_{c0} = 0.0022$.

The T-specimen is modelled by three modified flexibility-based elements, one element for

Table 1 Maximum loading capacity of the specimens and torsional capacity of the spandrel beams in Hsu and Burton (1974) and Collins and Lampert (1971) tests

	Maximum loading capacity of specimen (kN)				Torsional capacity of spandrel beam (kN·m)				Failure mode			
	A3	B2	S1	S3	A3	B2	S1	S3	A3	B2	S1	S3
Experiment	151	126	248	292	5.35	4.54	77.5	111.5	F[#]	F[#]	F[#]	S[##]
Present study	156	124	232	278	5.55	4.73	75.1	103.1	F[#]	F[#]	F[#]	F-S[*]

[*]Flexural-shear failure
[#]Flexural failure
[##]Shear failure

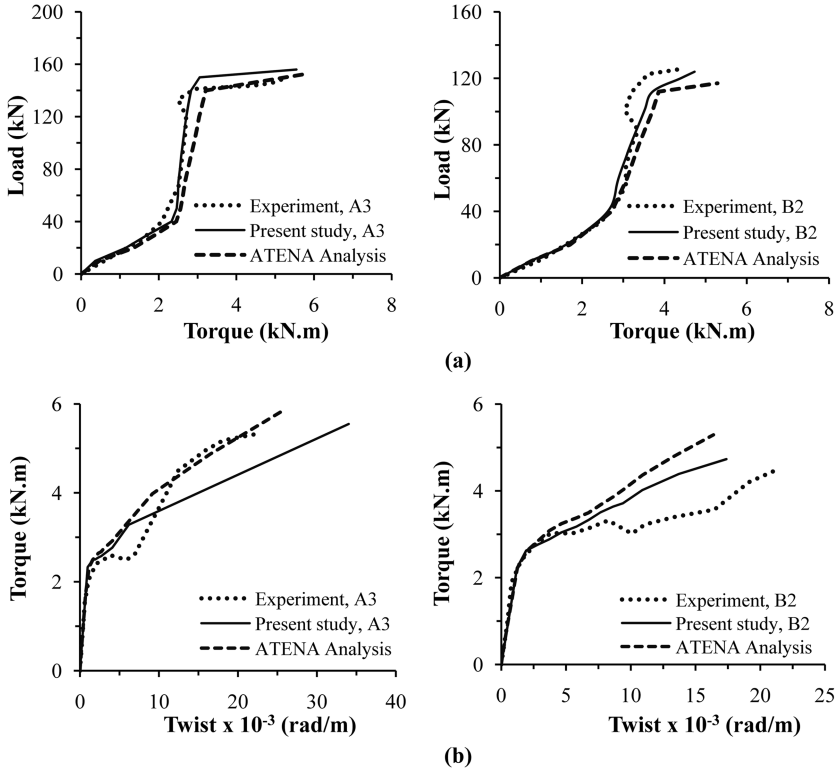

Fig. 8 (a) Load versus spandrel beam torque, (b) torque versus twist of the spandrel beam for specimens A3 and B2 in Hsu and Burton (1974) test

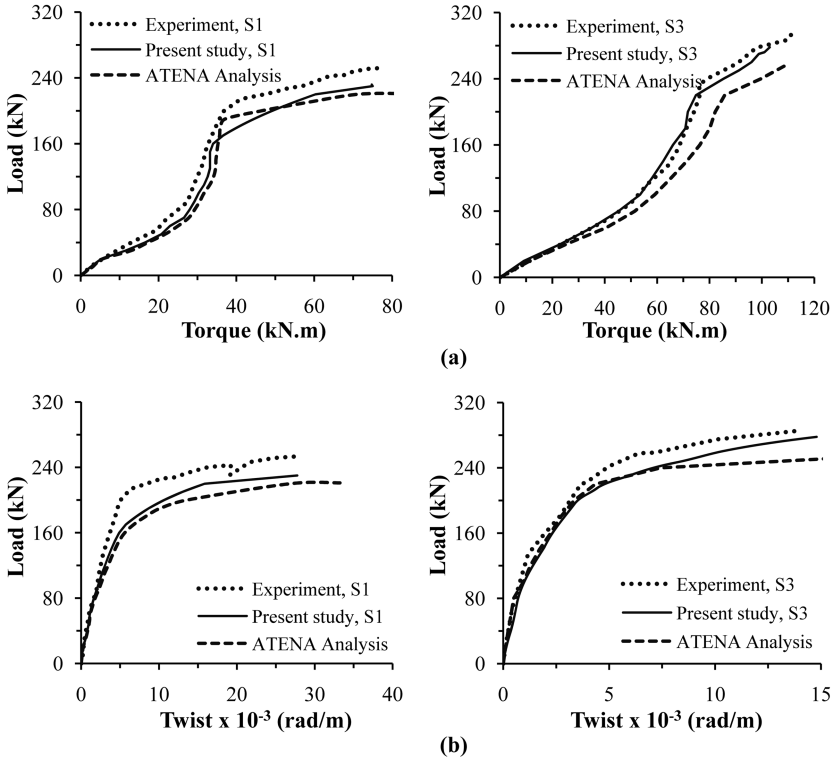

Fig. 9 (a) Load versus torque imposed at the mid-span of the spandrel beam, (b) load versus twist of the spandrel beam for specimens S1 and S3 in Collins and Lampert (1971) test

modelling of the floor beam and two elements to represent each half of the spandrel beam. A composite Simpson's method with 19 integration points over both section depth and width is used in the analytical model and the distance between longitudinal integration points is limited to 200 mm.

The maximum loading capacity of the specimens, torsional capacity of the spandrel beams and failure mode of different specimens obtained from the analytical model are compared with the experimental data in Table 1. The load versus spandrel beam torque and the torque versus twist of the spandrel beams for specimens A3 and B2 are shown in Fig. 8 and the load versus torque imposed at the mid-span of the spandrel beam and the load versus twist of the spandrel beam for specimens S1 and S3 are shown in Fig. 9. It is observed that the results of the analytical model correlate well with the experimental results. Furthermore, in order to show the efficiency and accuracy of the proposed model compared with more expensive continuum-based finite element models, the T-specimens are modelled in ATENA-3D (Cervenka *et al*. 2002). In ATENA, the 3D Nonlinear Cementitious Material model, which is basically a fracture-plastic constitutive law, is used for modelling concrete behaviour and discrete reinforcement with a linear elastic-hardening 1D stress-strain relationship employed to model the longitudinal and transverse steel bars (Cervenka *et al*. 2005). The relative size of the brick elements used in ATENA model is limited to 30 mm for specimen A3 and B2 and 50 mm for specimens S1 and S3.

The total analysis time for the model with frame elements to construct the equilibrium path with

10 unequal load steps was less than 3.2 seconds for all of the specimens, compared with 674 seconds for the ATENA model. This demonstrates the efficiency of the formulation developed in this study. The average number of iterations required for convergence of flexibility frame model varies from 6 to 11 iterations at different loading stages.

8.3 Progressive collapse test of a 5-bay, 3-storey RC frame

In this example the potential progressive collapse of a 3-storey building, of plan and reinforcing details shown in Fig. 10, is studied. The storey height is $h = 3.4$ m and the structure has been designed based on the AS3600 (2009) for a dead load of $G = 5$ kN/m^2, including structure self-weight, perimeter wall load of $G = 5$ kN/m, live load of $Q = 3.0$ kN/m^2 and a uniform lateral wind pressure of $W = 1.2$ kN/m^2.

The material properties are $f_y = 400$ MPa, $E_s = 2.0 \times 10^5$ MPa, $f_{cp} = 28$ MPa, $E_0 = 2.8 \times 10^4$ MPa and $f_t = 2.0$ MPa. The concrete strain corresponding to compressive strength of unconfined concrete is $\varepsilon_{c0} = 0.002$ and the ultimate strain of unconfined compressive concrete is $\varepsilon_{cu} = 0.01$. The effect of confinement on the concrete strength and stiffness is considered by adopting the Mander *et al.* (1988) model.

In the model, each column and each beam in the *y*-*y* direction is modelled with 1 element and in *x*-*x* direction each beam consists of 3 elements. The section of column is divided to 17 fibres over

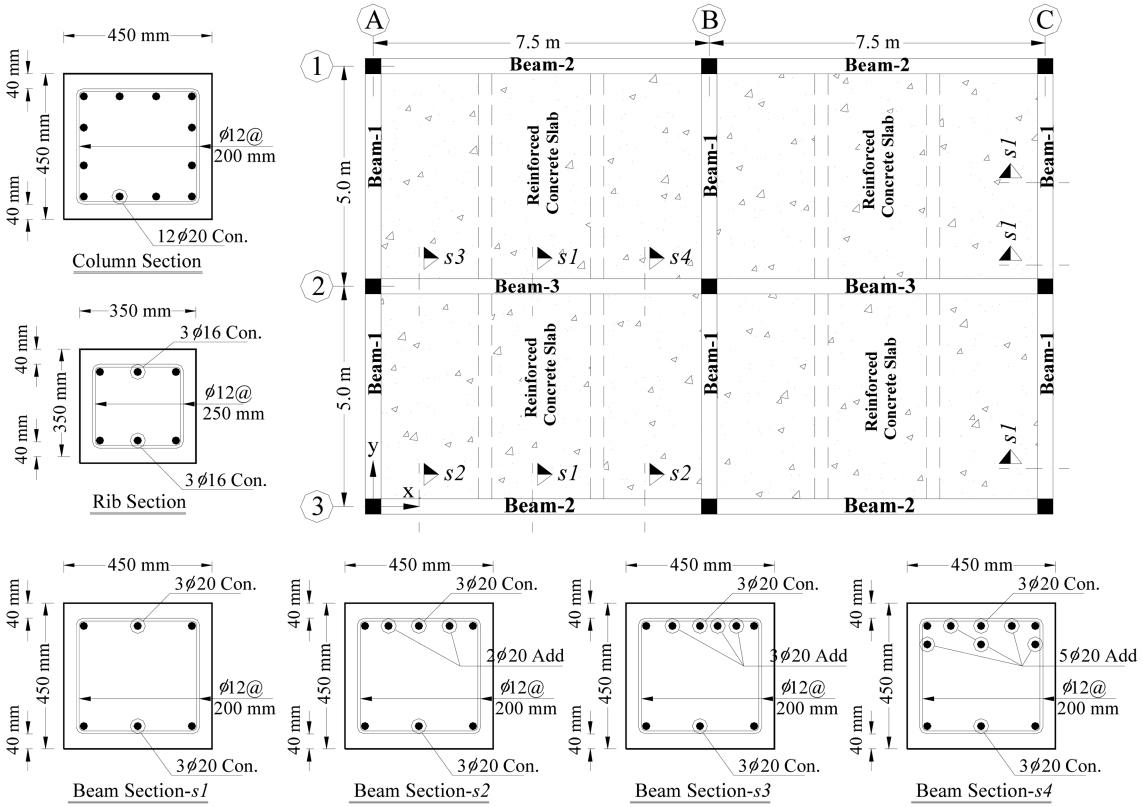

Fig. 10 Plan of the 3-storey building and the sections reinforcing details

both depth and width and for beams the section is divided to 19 fibres over depth and 13 fibres over width. The distance between longitudinal integration points varies between 250 mm to 300 mm.

The load combination considered for progressive collapse assessment includes the dead load plus 25% of the live load, which is consistent with GSA (2003) provisions. First a static analysis for the structure under a load combination of G + 0.25 Q was carried out and the internal nodal forces on the top of the columns B-1, C-1 and C-2 were determined. In the next step, three scenarios were considered. In scenario-1 column B-1 is removed, in scenario-2 column C-1 is removed and in scenario-3 column C-2 is removed. For each scenario, nodal forces of the removed columns are imposed on the top joints with opposite sign. These nodal forces are then removed over a period of 1 msec and the ensuing dynamic response of the structure, under the load combination G+0.25Q, captured.

The Newmark scheme with a maximum time step of 4 msec was used for the dynamic analysis. Adopting a Rayleigh damping, with a mass and initial stiffness multiplier of $a = b = 0.001$ (equivalent to modal damping factors of $\zeta_1 = 0.004$ and $\zeta_4 = 0.008$ for the first and fourth modes), the history of vertical displacement for joints B-1 and C-1 on the first level corresponding with scenario-1 and scenario-2, is given in Fig. 11. With regard to the AS3600 (2009) provisions for linear elastic analyses, the column bending stiffness were multiplied by 0.8 and the beams bending and torsional stiffnesses were multiplied by a factor of 0.4. Comparing the maximum displacement obtained from a dynamic analysis with that of the static analysis results suggests a dynamic load factor (*DLF*) of the order of 1.8 to 2.0 for linear and a *DLF* between 1.3 and 1.6 for nonlinear analysis which is consistent with the commonly accepted dynamic load factor of 2 as accepted in various design manuals (GSA 2003, US DoD 2004). Furthermore, the *DLF* for different scenarios is reported in Table 2.

In Fig. 12, the dynamic history of the vertical displacement for scenario-1 and scenario-2, with and without damping and including linear (initial) and nonlinear torsional stiffness, are compared to show the importance of damping and torsion on the nonlinear dynamic response of the structure. It is noteworthy that adopting a reasonable value for the damping factor can improve the stability of the numerical analysis, removing the noise from the response and resolving some convergence issues. With regard to Fig. 12, it is observed that the difference between maximum displacements predicted by models with linear torsion (l/torsion) and nonlinear torsion (nl/torsion) is less than 8%

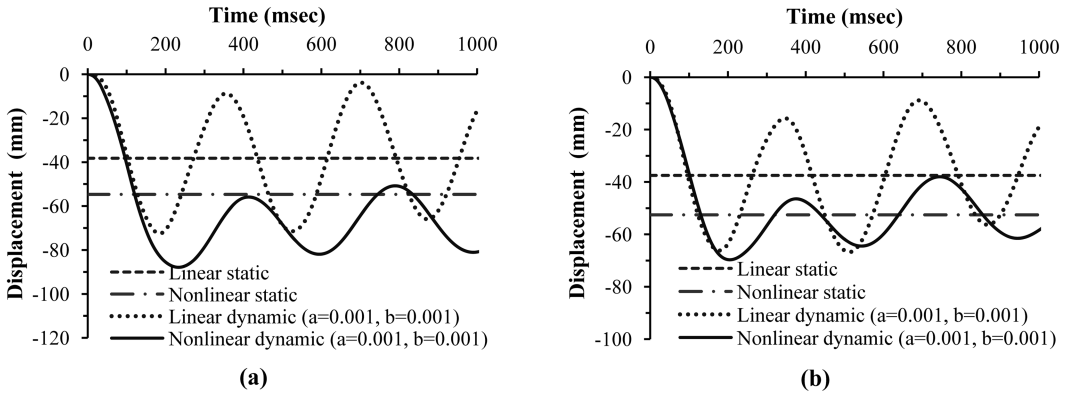

Fig. 11 History of vertical displacement for joint (a) B-1 in the scenario-1, (b) C-1 in the scenario-2

Table 2 Maximum displacement obtained from different type of analysis and calculated *DLF* for different scenarios

	Maximum displacement from different analyses (mm)						
	Linear analysis		Non-linear analysis			*DLF* (with damping)	
	Static	Dynamic	Static	Dynamic		Linear analysis	Nonlinear analysis
				n/l torsion	l/ torsion		
Scenario-1	38.2	72.5	54.7	87.9	79.5	1.88	1.61
Scenario-2	37.5	66.2	52.5	69.7	65.0	1.77	1.33
Scenario-3	29.6	59.3	40.2	51.9	49.0	2.00	1.29

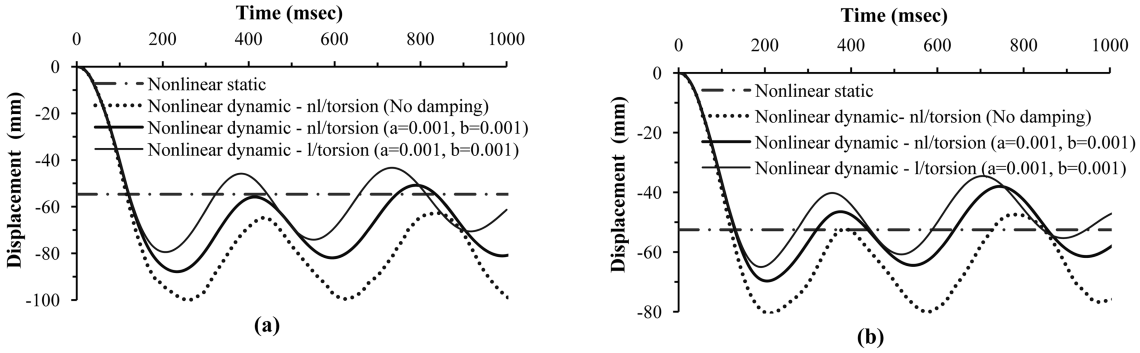

Fig. 12 Effect of damping and variable torsional stiffness on the history of vertical displacement for joint (a) B-1 in the scenario-1, (b) C-1 in the scenario-2

in this example and it can be concluded that the torsional response of elements has only a minor effect on the global response of the structure. The total time of analysis for the linear, non-linear with linear torsion and non-linear with non-linear torsion on a PC with a 3.0 GHz dual-core processor and running Windows Vista are 0.6, 69 and 95 minutes, respectively.

8.4 Potential progressive collapse analysis of a 6-storey frame

In this example, progressive collapse analysis of the 6-storey building shown in Fig. 13 is presented. The storey height is $h = 3.2$ m and the building was designed using the principles of AS3600 (2009) for a dead load of $G = 5$ kN/m^2, perimeter wall load of $G = 5$ kN/m, live load of $Q = 2.0$ kN/m^2 and a uniform lateral wind load of $W = 1.5$ kN/m^2. The material properties are: $f_y = 400$ MPa, $E_s = 2.0 \times 10^5$ MPa, $f_{cp} = 30$ MPa, $E_0 = 3.0 \times 10^4$ MPa and $f_t = 2.1$ MPa. The concrete strain corresponding to compressive strength of unconfined concrete was $\varepsilon_{c0} = 0.0022$ and the ultimate strain of unconfined compressive concrete was taken as $\varepsilon_{cu} = 0.01$.

In the analytical model, each column was modelled with 1 element with 21 fibres over both the section depth and width. Each beam in *x*-*x* direction was modelled with 1 element and in the *y*-*y* direction 3 elements were used. For the beams, the section depth and width are divided to 19 and 13 fibres, respectively. The distance between longitudinal integration points varies between 280 mm to 310 mm.

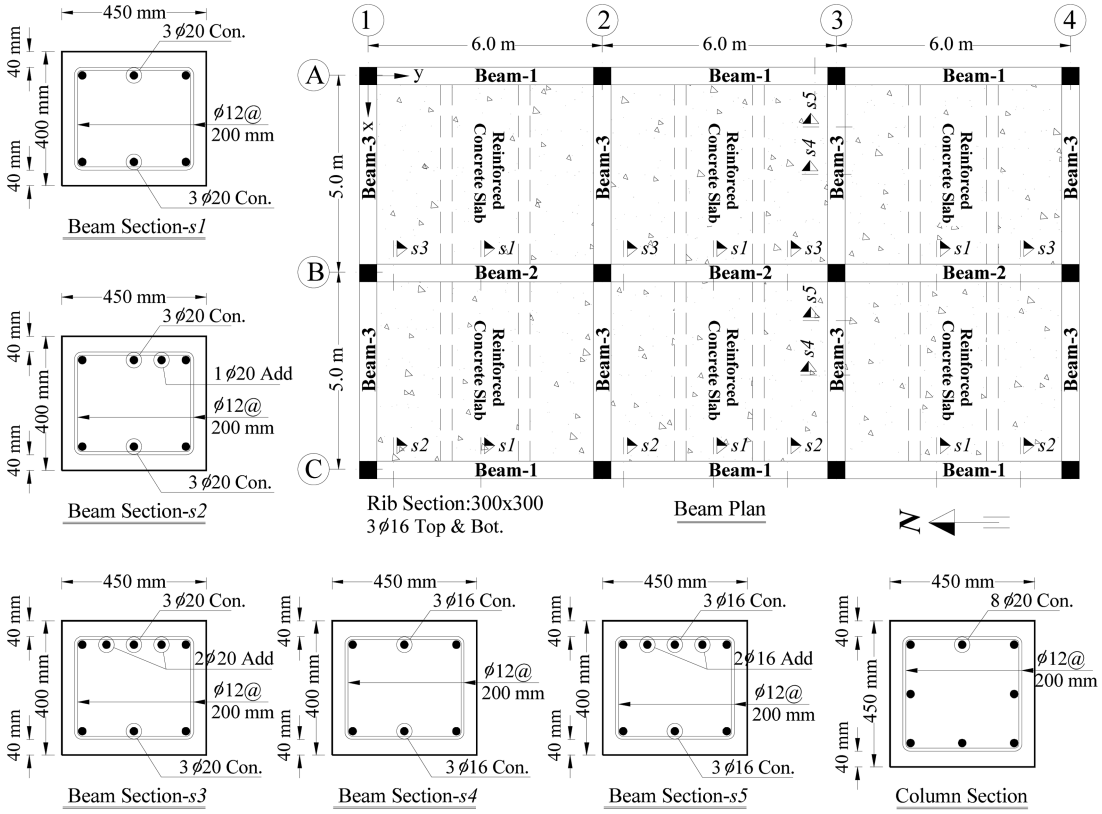

Fig. 13 Plan of the 6-storey building and the sections reinforcing details

The load combination considered for progressive collapse assessment was G + 0.25 Q. Two scenarios based on instantaneous removal of columns C-1 (scenario-1) and C-2 (scenario-2) on the ground floor are studied. The procedure for the progressive collapse analysis is as per that used in the previous example.

The Newmark scheme with variable time steps and a maximum time step of 4 msec was used for the dynamic analysis. Adopting a Rayleigh damping with a mass and initial stiffness multiplier of $a = b = 0.001$ (equivalent to modal damping factors of $\zeta_1 = 0.003$ and $\zeta_8 = 0.015$ for the first and eighth modes), the history of vertical displacement for joints C-1 and C-2 on the first level and corresponding with each scenario are monitored. The results from the nonlinear dynamic analysis and from a linear elastic analysis are plotted in Fig. 14. For the linear analysis, the effective stiffness was taken as 0.4 times the gross stiffness for the beams, and 0.8 times the gross stiffness for the columns. Comparing the maximum displacement obtained from a dynamic analysis with static results shows a *DLF* of 1.7 and 1.9 for scenario-1 and 2, respectively, which is consistent with the value of *DLF* = 2 as adopted in various design manuals (GSA 2003, US DOD 2004).

In Fig. 15, the history of displacements is plotted for scenarios 1 and 2 with two different levels of damping and for the cases of linear and nonlinear torsion. It is noteworthy that adopting high levels of damping may underestimate the displacement response of the structure, which is not the case for linear elastic analysis. With regard to Fig. 15, it is observable that the difference between

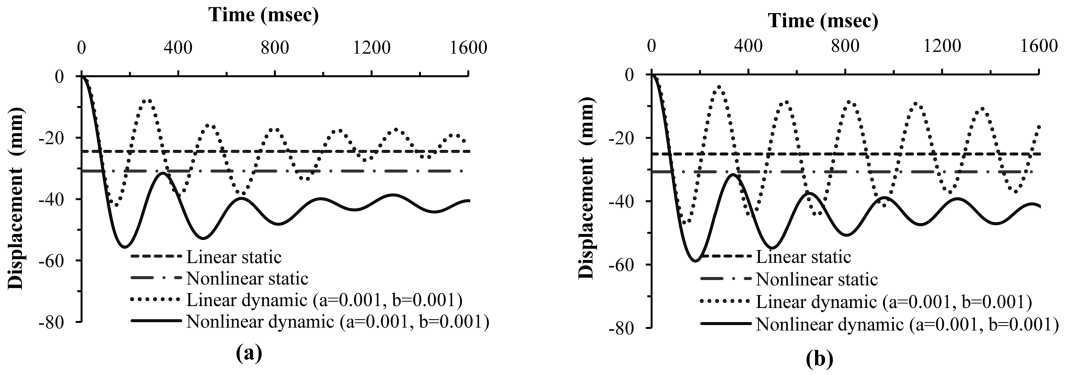

Fig. 14 History of vertical displacement for joint (a) C-1 in the scenario-1, (b) C-2 in scenario-2

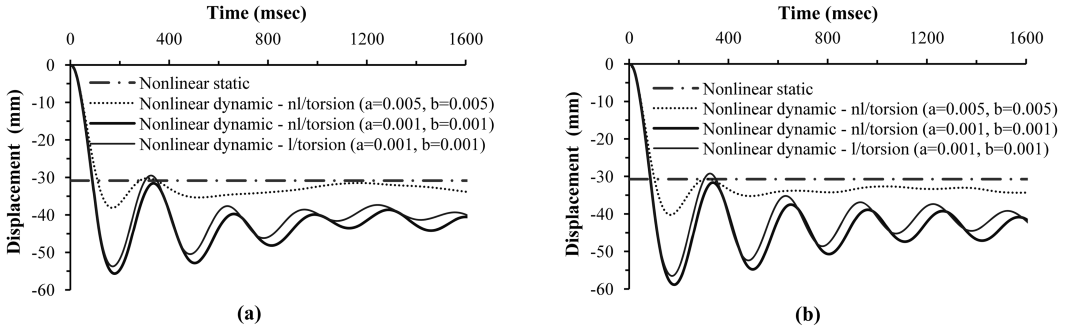

Fig. 15 Effect of damping and variable torsional stiffness on the history of vertical displacement for joint (a) C-1 in the scenario-1, (b) C-2 in the scenario-2

maximum displacements predicted by models with linear torsion (l/torsion) and nonlinear torsion (nl/torsion) is less than 5% in this example and it can be concluded that the torsional response of elements has only a minor effect on the global response. The total time of analysis for the linear model, nonlinear model with linear torsion and nonlinear model with nonlinear torsion on a PC with a 3.0 GHz dual-core Intel processor and running Windows Vista was 1.1, 178 and 283 minutes, respectively.

8.5 3D model of a 3-storey 1-bay frame

In this final example, the behaviour of a 3-storey building analysed by Shi *et al.* (2008) using LS-DYNA is studied. The plan of the building and outline of the model prepared in LS-DYNA are shown in Fig. 16. The storey height is $h = 3.0$ m and dimensions of all columns are 300 × 300 mm beams 200 × 300 mm all with 2% longitudinal reinforcement with yield stress of $f_y = 335$ MPa and 10 mm diameter hoop reinforcement at 200 mm spacings with the yield stress of $f_{yh} = 235$ MPa. The slab is 150 mm thick with 2% longitudinal reinforcement in each direction (1% in each layer). The weight of the infill walls was taken as 0.8 kN/m^2 and live load is $Q = 4.0$ kN/m^2.

The load combination used for progressive collapse assessment is G + 0.25 Q according to GSA (2003) and a progressive collapse assessment is undertaken with the removal of the middle ground

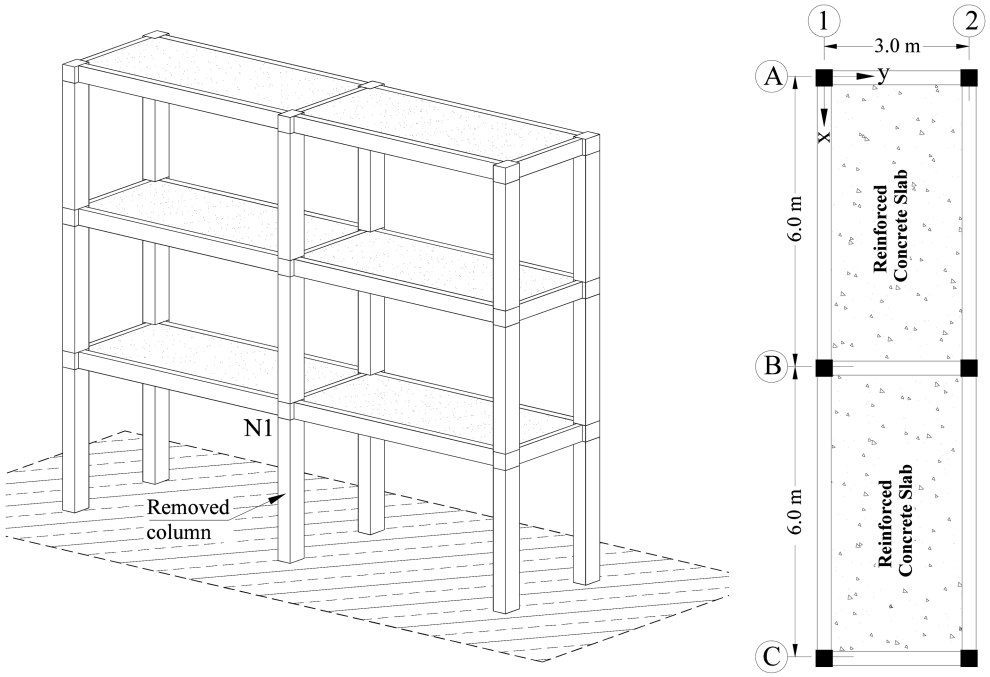

Fig. 16 Plan and outline of the 3-storey building model in LS-DYNA (Shi *et al*. 2008)

floor column. The properties of concrete were taken as $f_{cp} = 32$ MPa, $f_t = 2.0$ MPa, $\varepsilon_{c0} = 0.002$ and $\varepsilon_{cu} = 0.01$. The strain rate effects on the concrete and steel bars behaviour are taken into account using the dynamic increase factor approach (Valipour *et al*. 2009).

For the LS-DYNA analysis, the concrete was modelled using MATERIAL 72 and steel bars with MATERIAL 003. The strain rate effect was taken into account and 3D solid elements with a size of 50 mm on each side were used (Shi *et al*. 2008).

In the frame model, each column is modelled with 1 element with 11 Simpson integration points along the element axis. In the *y*-*y* direction, each beam is modelled with 1 element with 13 integration points along the element axis and in the *x*-*x* direction, each beam consists of 4 equal elements with and 9 integration points along each element. Further, the section depth and width are divided to 11 fibres and nonlinear torsion model is adopted within 3D frame model. Each bay of the one-way slab is modelled by 3 equivalent beams of 1500 mm width and 150 mm depth and the remaining part of slab thickness is considered as a flange for the beams in *y*-*y* direction. For the dynamic analysis, the Newmark scheme with a maximum time step of 5 msec is used with Rayleigh damping with the mass and initial stiffness multipliers of $a = b = 0.001$.

The history of vertical displacement and velocity for joint N1 after removal of the middle column (B-1) is shown in Fig. 17. The maximum displacement of joint N1 obtained from the frame model is 208 mm, which is close to the value of 234 mm predicted by the LS-DYNA analysis. In general, the correlation between the LS-DYNA and frame models for predicting the global response of the structure is reasonable. The LS-DYNA model, however, can potentially capture local effects of 3D stress state on the material response as well as the higher modes of deformation, which the frame element is incapable of predicting.

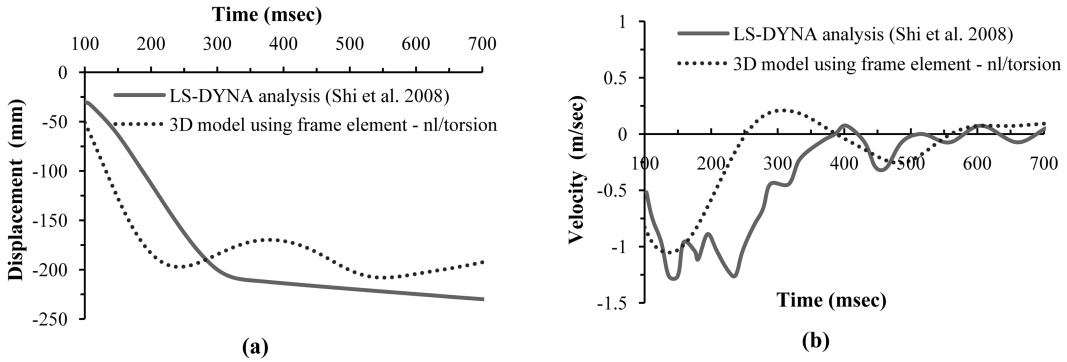

Fig. 17 History of (a) vertical displacement, (b) vertical velocity of joint N1

The total time of analysis for the 3D frame model on a PC with a 3.0 GHz dual-core Intel processor and running Windows Vista was just 140 seconds, which is comparable with the computation time (approximately 5 minutes) for an explicit procedure such as that used in the LS-DYNA solver.

9. Conclusions

The formulation of a nonlinear reinforced concrete frame element including torsion is derived. The formulation takes both physical and second order geometrical nonlinearities into account.

The developed frame element is used for static and dynamic progressive collapse assessment of 3D reinforced concrete frames based on the alternate load path method and it is shown that the element is computationally very efficient while maintaining good accuracy. Furthermore, by comparing the maximum displacements predicted by models with linear torsion (l/torsion) and nonlinear torsion (nl/torsion) it was shown that the torsional behaviour of reinforced concrete elements satisfying minimum standard requirements is not significant for progressive collapse assessment of the framed structures studied.

Different levels of damping were used for progressive collapse analysis and it was shown that adopting a reasonable value of damping for nonlinear dynamic analysis of frames improves the numerical stability and can avoid an underestimation of displacements.

Comparing the results of nonlinear static and dynamic analysis, the dynamic to static ratio of maximum displacement was estimated and it was shown that the impact load factor of 2 adopted by different guidelines, for example GSA (2003), to take account of the dynamic effects in an equivalent static analysis, provides a reasonably conservative upper bound for the studied cases.

The importance of nonlinear analysis for progressive collapse assessment of frames was demonstrated by comparing linear and nonlinear dynamic analysis results. Finally, it was demonstrated that the stable implicit modelling approach developed in this thesis, combined with the efficient model formulation, could have a similar computational efficiency as the, conditionally stable, explicit formulations currently available.

References

ACI 318-99 (1999), *Building Code Requirements for Structural Concrete and Commentary*, American Concrete Institute, Farmington Hills, MI.
CEB-FIP Model Code 1990: Design Code (1993), Thomas Telford, London.
AS3600-2009 (2009), *Australian Standard, Concrete Structures*.
Bairan, J.M. and Mari, A.R. (2007), "Multiaxial-coupled analysis of RC cross-sections subjected to combined forces", *Eng. Struct.,* **29**(8), 1722-1738.
Bao, Y., Kunnath, S.K., El-Tawil, S. and Lew, H.S. (2008), "Macromodel-based simulation of progressive collapse: RC frame structures", *J. Struct. Eng.,* **134**(7), 1079-1091.
Bathe, J.K. (1997), *Finite Element Procedures,* McGraw Hill, New York.
Carol, I. and Murcia, J. (1989), "Nonlinear time-dependent analysis of planar frames using an 'exact' formulation. I. Theory", *Comput. Struct.,* **33**(1), 79-87.
Cervenka, V., Cervenka, J. and Pukl, R. (2002), "ATENA - A tool for engineering analysis of fracture in concrete", *Sadhana - Academy Proceedings in Engineering Sciences,* **27**(4), 485-492.
Cervenka, V., Jendele, L. and Cervenka, J. (2005), "ATENA program documentation, Part 1: theory", Prague.
Coleman, J. and Spacon, E. (2001), "Localization issues in force-based frame elements", *J. Struct. Eng.-ASCE,* **127**(11), 1257-1265.
Collins, M.P. and Lampert, P. (1971), "Redistribution of moments at cracking- the key to simpler torsion design", Department of Civil Engineering, University of Toronto, Toronto.
Cornelissen, H.A.W., Hordjik, D.A. and Reinhardt, H.W. (1986), "Experimental determination of crack softening characteristics of normal weight and lightweight concrete", *Heron,* **31**(2), 45-56.
DoD (2005), *Design of Building to Resist Progressive Collapse*, Washington DC.
Ellingwood, B. and Leyendecker, E.V. (1978), "Approaches for design against progressive collapse", *J. Struct. Eng.-ASCE,* **104**(ST3), 413-423.
Gong, S., Lu, Y., Tu, Z. and Jin, W. (2009), "Validation study on numerical simulation of RC response to close-in blast with a fully coupled model", *Struct. Eng. Mech.,* **32**(2), 283-300.
GSA (2003), *Progressive Collapse Analysis and Design Guidelines for New Service Administration*, Washington DC.
Hsu, T.T.C. (1984), *Torsion of Reinforced Concrete,* Van Nostrand Reinhold, New York.
Hsu, T.T.C. and Burton, K.T. (1974), "Design of reinforced concrete spandrel beams", *J. Struct. Div.,* **100**(1), 209-229.
Izzuddin, B.A., Vlassis, A.G., Elghazouli, A.Y. and Nethercot, D.A. (2008), "Progressive collapse of multi-storey buildings due to sudden column loss - Part I: Simplified assessment framework", *Eng. Struct.,* **30**(5), 1308-1318.
Kaewkulchai, G. and Williamson, E.B. (2004), "Beam element formulation and solution procedure for dynamic progressive collapse analysis", *Comput. Struct.,* **82**(7-8), 639-651.
Khandelwal, K., El-Tawil, S., Kunnath, S.K. and Lew, H.S. (2008), "Macromodel-based simulation of progressive collapse: Steel frame structures", *J. Struct. Eng.,* **134**(7), 1070-1078.
Kim, J. and Park, J. (2008), "Design of steel moment frames considering progressive collapse", *Steel Compos. Struct.,* **8**(1), 85-98.
Klus, J.P. (1968), "Ultimate strength of reinforced concrete beams in combined torsion and shear", *Am. Concrete Inst. J.,* **65**(3), 210-216.
Lampert, P. and Thurlimann, B. (1968), "Torsionsversuche an stahlbetonbalken, (Torsion test of reinforced concrete beams)", Report No. Nr 6506-2, Institute Fur Baustatik, ETH Zurich (in German), Zurich.
Mander, J.B., Priestley, M.J.N. and Park, R. (1988), "Theoretical stress-strain model for confined concrete", *J. Struct. Eng.,* **114**(8), 1804-1826.
Mitchell, D. and Collins, M.P. (1974), "The behavior of structural concrete beams in pure torsion", Report No. 74-06, Department of Civil Engineering, University of Toronto, Toronto.
Mohamed, O.A. (2009), "Assessment of progressive collapse potential in corner floor panels of reinforced concrete buildings", *Eng. Struct.,* **31**(3), 749-757.
Navarro Gregori, J., Miguel Sosa, P., Fernandez Prada, M.A. and Filippou, F.C. (2007), "A 3D numerical model

for reinforced and prestressed concrete elements subjected to combined axial, bending, shear and torsion loading", *Eng. Struct.,* **29(**12), 3404-3419.
Rahal, K.N. and Collins, M.P. (1996), "Simple model for predicting torsional strength of reinforced and prestressed concrete sections", *ACI Struct. J.,* **93**(6), 658-666.
Sasani, M. (2008), "Response of a reinforced concrete infilled-frame structure to removal of two adjacent columns", *Eng. Struct.,* **30**(9), 2478-2491.
Sasani, M. and Kropelnicki, J. (2008), "Progressive collapse analysis of an Rc structure", *Struct. Des. Tall Spec.,* **17**(4), 757-771.
Sasani, M. and Sagiroglu, S. (2008a), "Progressive collapse of reinforced concrete structures: A multihazard perspective", *ACI Struct. J.,* **105**(1), 96-103.
Sasani, M. and Sagiroglu, S. (2008b), "Progressive collapse resistance of hotel San Diego", *J. Struct. Eng.,* **134**(3), 478-488.
Shi, Y., Hao, H. and Li, Z. (2008), "An improved procedure for progressive collapse analysis of RC frames to blast loading", *Blast Design and Modelling Forum.* Canberra.
Valipour, H.R. (2009), "Nonlinear analysis of reinforced concrete frames under extreme loadings", PhD Dissertation, School of Civil and Environmental Engineering, The University of New South Wales, Sydney, Australia.
Valipour, H.R. and Foster, S.J. (2008), "A total secant flexibility-based formulation for frame elements with physical and geometrical nonlinearities", *Finite Elem. Anal. Des.*, (submitted for publication).
Valipour, H.R. and Foster, S.J. (2009a), "Non-local damage formulation for a flexibility-based frame element", *J. Struct. Eng.-ASCE,* **135**(10), 1213-1221.
Valipour, H.R. and Foster, S.J. (2009b), "Nonlinear reinforced concrete frame element with torsion", *J. Eng. Struct.*, (submitted for publication).
Valipour, H.R., Huynh, L. and Foster, S.J. (2009), "Analysis of RC beams subjected to shock loading using a modified fibre element formulation", *Comput. Concrete,* **6**(5), 377-390.
Valipour, H.R. and Foster, S.J. (2010), "A Total secant flexibility-based formulation for frame elements with physical and geometrical nonlinearities", *Finite Elem. Anal. Des*., **46**(3), 288-297.
Valipour, H.R. and Foster, S.J. (2010), "Nonlinear reinforced concrete frame element with torsion", *J. Eng. Struct*., **32**(4), 988-1002.
Vecchio, F.J. and Collins, M.P. (1986), "Modified compression-field theory for reinforced concrete elements subjected to shear", *J. Am. Concrete. Inst.,* **83**(2), 219-231.
Weerheijm, J., Mediavilla, J. and Van Doormaal, J.C.A.M. (2009), "Explosive loading of multi storey RC buildings: Dynamic response and progressive collapse", *Struct. Eng. Mech.,* **32**(2), 193-212.
Yagob, O., Galalf, K. and Naumoski, N. (2009), "Progressive collapse of reinforced concrete structures", *Struct. Eng. Mech.,* **32**(6), 771-786.
Yi, W.J., He, Q.F., Xiao, Y. and Kunnath, S.K. (2008), "Experimental study on progressive collapse-resistant behavior of reinforced concrete frame structures", *ACI Struct. J.,* **105**(4), 433-439.
Young, W.C. and Roark, R.J. (2001), *Roark's Formulas for Stress and Strain*, McGraw-Hill Professional.